ACS OMEGA

Article

Cite This: ACS Omega 2019, 4, 9996−10002

http://pubs.acs.org/journal/acsodf

High-Performance Hybrid Photovoltaics with Efficient Interfacial Contacts between Vertically Aligned ZnO Nanowire Arrays and Organic Semiconductors

Yoon Ho Lee,[†,#,§,∥] Minjeong Ha,[‡,§] Inho Song,[†] Jeong Hun Lee,[†] Yousang Won,[†] Seongdong Lim,[‡] Hyunhyub Ko,[*,‡] and Joon Hak Oh[*,†]

[†]School of Chemical and Biological Engineering, Institute of Chemical Processes, Seoul National University, 1 Gwanak-ro, Gwanak-gu, Seoul 08826, Republic of Korea

[#]Center for Advanced Soft Electronics, Pohang University of Science and Technology (POSTECH), Pohang 37673, Gyongbuk, Republic of Korea

[‡]School of Energy and Chemical Engineering, Ulsan National Institute of Science and Technology (UNIST), Ulsan 44919, Republic of Korea

Supporting Information

ABSTRACT: Hybrid photovoltaics (HPVs) incorporating both organic and inorganic semiconducting materials have attracted much attention as next-generation photovoltaics because of their advantage of combining both materials. The hybridization of ZnO nanowires (NWs) and organic semiconductors is expected to be a suitable approach to overcome the limited exciton diffusion length and low electron mobility associated with current organic photovoltaics. The use of ZnO NWs allows researchers to tune nanoscale dimensions more precisely and to achieve rod-to-rod spacing below 10 nm. However, the perfect incorporation of organic semiconductors into densely packed ZnO NW arrays has yet to be achieved. In this study, we report the fabrication of ZnO NW arrays and various organic heterojunction-based HPVs using the feasible and effective vacuum-assisted double coating (VADC) method, achieving full coverage of the organic semiconductors on the compact ZnO NW arrays. The newly proposed VADC method ensures perfect infiltration and full coverage of the organic semiconductors on the densely packed NW arrays. Compared with the conventional single spin-coating process, the use of the VADC method led to 11 and 14% increases in the power conversion efficiency of P3HT:PCBM- and PBDTTT-C-T:$PC_{71}BM$-based HPVs, respectively. Our studies provide a feasible method for the fabrication of efficient HPVs.

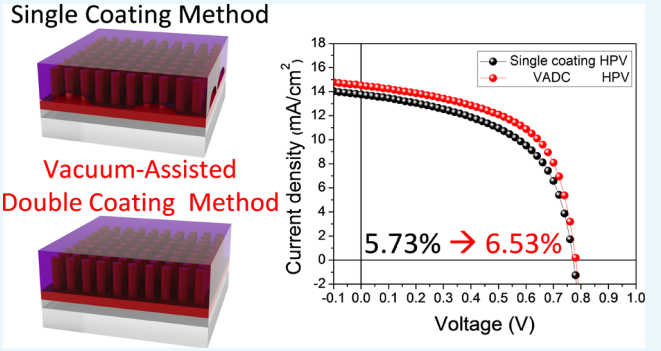

1. INTRODUCTION

Organic semiconductor-based photovoltaics (OPVs) have attracted a great deal of attention for their use in next-generation photovoltaics because of their potential advantages including light weight, mechanical flexibility, and low-cost fabrication over a large area.[1−4] Although the performance of OPVs has been rapidly improved by molecular design,[4,5] crystallinity and morphology control,[6,7] and the introduction of light trapping structures,[8,9] OPVs still have the limitation of short exciton diffusion lengths (several tenths of nanometers) compared with inorganic material-based photovoltaics (PVs).[2,10,11] An exciton diffusion bottleneck of conjugated polymers results in photogenerated excitons failing to reach the donor/acceptor interface. This causes the recombination of excitons and is a limitation of OPV efficiencies. Moreover, organic semiconductors show intrinsically low-charge carrier mobilities and limited stability under ambient conditions, which limits the performance of OPVs.[12−14]

To overcome these limitations, the inverted design of hybrid photovoltaics (HPVs) incorporating both organic/inorganic semiconducting materials has been introduced extensively. The synergistic effect of both the organic/inorganic materials present within the hybrid system has seen improvements in both device performance and stability.[15−21] For an efficient hybrid system, the use of ZnO nanowires (NWs) as the inorganic component within the HPV is an attractive prospect.[22−24] ZnO NWs are easily fabricated using a low-cost solution process and possess a large surface area.[25−30] In addition, the nanoscale dimensions are tunable, allowing rod-to-rod spacing below 10 nm.[28] It is anticipated that incorporating highly ordered ZnO NWs within the organic bulk heterojunction (BHJ) will result in a large increase in the

Received: March 21, 2019
Accepted: May 23, 2019
Published: June 7, 2019

interfacial area; this is expected to solve the limits about short exciton diffusion lengths and low electron mobilities observed with OPVs.[22,31−36] In addition, the inverted structure of HPVs, fabricated by coating the top anodes with high work-function metals such as Au, Ag and Cu, can play an important role in overcoming the limited device stability of HPVs.[37−41] Despite the benefits of combining organic semiconductors with ZnO NWs for HPVs, inefficient infiltration and partial interfacial contact between the organic semiconductors and densely packed ZnO NWs has been found to reduce the performance of HPVs.[31,42,43] Therefore, to improve the performance of HPVs, novel methods of fabricating an ideal hybrid film, in which organic semiconductors are completely incorporated into ZnO NWs, are needed. This will further improve our understanding of their photophysical properties and the extent to which these systems can be used in practical applications.

In this study, we introduce the vacuum-assisted double coating (VADC) method for the perfect infiltration and full interfacial contact of poly(3-hexylthiophene) (P3HT):[6,6]-phenyl C_{61}-butyric acid methyl ester (PCBM), poly((4,8-bis-(2-ethyl-hexyl-thiophene-5-yl)-benzo[1,2-*b*,4,5-*b*′]-dithiophene-2,6-diyl)-*alt*-(2-(2′-ethyl-hexanoyl)-thieno[3,4-*b*]-thiophen-4,6-diyl)) (PBDTTT-C-T):[6,6]-phenyl-C_{71}-butyric acid methyl ester ($PC_{71}BM$) and ZnO NWs. We selected these organic materials for HPVs to demonstrate that the VADC method can be applied to the processing of a variety of organic semiconductor materials. P3HT:PCBM is the most widely used material in OPVs that require additional annealing processes, and PBDTTT-C-T:$PC_{71}BM$ is a highly efficient organic material for OPVs that do not require additional annealing.[44−46] The newly proposed VADC method greatly improved the infiltration of the organic semiconductors within the densely packed ZnO NW arrays, leading to 11 and 14% increases in the power conversion efficiency (PCE) of P3HT:PCBM- and PBDTTT-C-T:$PC_{71}BM$-based inverted HPVs, respectively, compared with the conventional single spin-coating method. Our studies provide an effective route to achieve ideal interfacial contact between the inorganic nanostructures and organic semiconductors, leading to an efficient heterojunction and higher HPV performance.

2. RESULTS AND DISCUSSION

The vertically aligned ZnO NW arrays with large surface areas and compact interspacing between NWs were uniformly grown on the surface of the glass/indium tin oxide (ITO)/ZnO substrates via a sol−gel process of the ZnO seed layer (∼50 nm in thickness) and further hydrothermal synthesis.[29,30] In addition, both the length and diameter of the ZnO NWs could be easily adjusted by changing the growth parameters such as temperature, time, and solution concentration. Figure 1a,b shows the typical top-view and cross-sectional scanning electron microscopy (SEM) images of the ZnO NW arrays, respectively. The vertically aligned ZnO NW arrays were grown at an optimized density and uniform length scale (100 ± 12 nm) and diameter (23 ± 1 nm). The crystallinity of hydrothermally grown ZnO NWs was also subjected to X-ray diffraction analysis (Figure 1c). X-ray diffraction patterns obtained from the ZnO NWs showed prominent peaks at 2θ of 31.7°, 34°, and 36°, corresponding to (100), (002), and (101) reflections, respectively. Although the hydrothermally grown ZnO NWs have slightly low crystalline peak intensity due to the limited growing time for molecular arrangement in ZnO

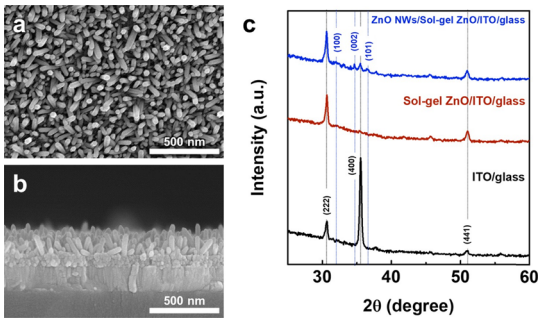

Figure 1. SEM images of the (a) top view and (b) cross-sectional view of ZnO NWs. (c) X-ray diffraction pattern of the glass/ITO/ZnO/ZnO NW substrate.

NWs, the peak patterns of as-synthesized ZnO NWs are matched perfectly with the crystalline index of references.

Initially, HPVs were fabricated using P3HT and PCBM as donor and acceptor materials, respectively, as they have been widely used over the past decade in OPV research. A schematic image with molecular structures of the organic semiconductors and energy diagram of the inverted HPVs consisting of glass/ITO/ZnO/ZnO NWs/P3HT:PCBM/MoO_3/Au are shown in Figure 2a,b, respectively (band gaps of P3HT and PCBM are ∼2.4 and ∼2 eV, respectively).[44,47] Due to the inverted structure of the HPVs, the electrical current flows inversely compared with conventional HPVs due to the utilization of high work-function Au electrodes that are more stable and improve cell stability. In this study, we used Au electrodes rather than Ag electrodes because of the high air stability due to the higher work function of Au electrodes compared to Ag electrodes,[48] although Ag electrodes were reported to show higher efficiency than gold electrodes due to their high reflectivity.[49] Moreover, photons can be effectively absorbed by either ZnO NWs or the organic BHJ layer.[34] To begin, using a conventional single spin-coating method, we fabricated HPVs by coating a P3HT:PCBM solution, dissolved in 1,2-dichlorobenzene (ODCB), onto 100 nm-long ZnO NWs that were present on a 50 nm-thick ZnO layer. The HPVs fabricated by this method exhibited a low PCE of 3.25% (Figure 3a and Table 1) due to imperfect infiltration of the organic solution into the densely packed ZnO NW arrays. The evidence of imperfect infiltration of the organic solution into the ZnO NW arrays was confirmed by SEM measurements. Figure 3b,c shows the SEM images before and after vacuum processing of the hybrid film fabricated by the conventional spin-coating method, respectively. It was confirmed that, upon applying vacuum treatment of the hybrid film, the interspatial voids between the organic layer and the ZnO NW layer was efficiently filled with the organic layer, resulting in the sinkage of the organic layer. The poor interfacial quality between the organic layer and inorganic nanostructures is a crucial issue for the PCE of HPVs, affecting both the photogenerated charge carrier collection and shunt resistance.[32,50] Thus, the level of infiltration of the organic layer into ZnO NWs determines the performance of the HPV systems.[31,51]

To overcome the infiltration problems observed by the single spin-coating method, we propose the use of the VADC method to remove interspatial voids at the organic/inorganic interface and two-step coating of the organic solution with different concentrations to help form a solid-state organic layer (Figure 4a). A diluted organic solution was spin-coated on the

DOI: 10.1021/acsomega.9b00778
ACS Omega 2019, 4, 9996−10002

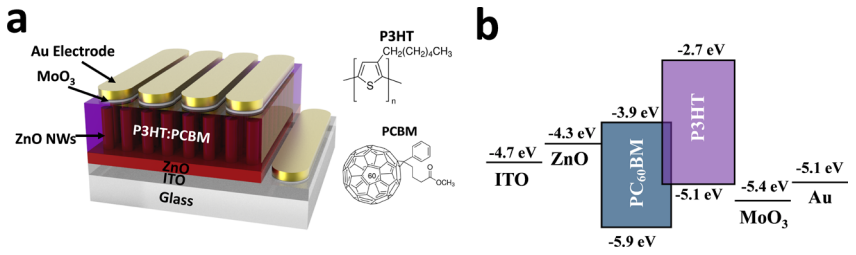

Figure 2. (a) Schematic image of the P3HT:PCBM-based HPV with molecular structures of P3HT and PCBM. (b) Schematic energy level diagram of the P3HT:PCBM-based HPV.

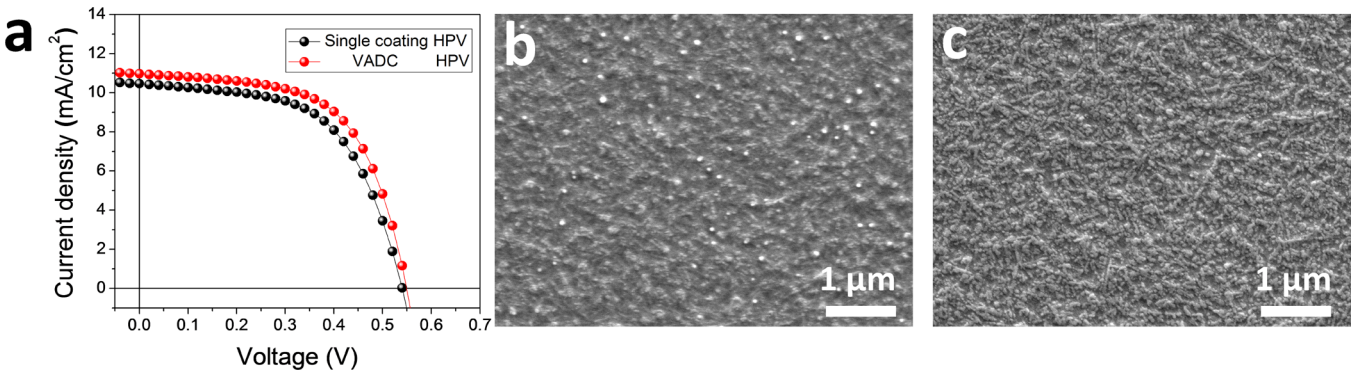

Figure 3. (a) J–V characteristics of P3HT:PCBM-based HPVs fabricated by the single spin-coating and VADC methods under white-light illumination (AM 1.5G, 100 mW/cm^2). (b, c) SEM images (b) before and (c) after vacuum processing of the hybrid film fabricated by the conventional spin-coating method.

Table 1. Photovoltaic Performance Parameters of the P3HT:PCBM-Based HPVs Fabricated Using the Single Spin-Coating and VADC Methods

coating methods	J_{sc} (mA/cm^2)	V_{oc} (V)	FF (%)	R_{sh} (KΩ cm^2)	R_s (Ω cm^2)	PCE$_{max}$ (PCE$_{av}$) (%)
single coating	10.5	0.54	57.5	4.25	16.9	3.25 (3.08)[a]
VADC	11.0	0.55	60.0	4.37	13.3	3.62 (3.48)

[a]Average values are based on the testing of five devices. R_{sh}, shunt resistance. R_s, series resistance.

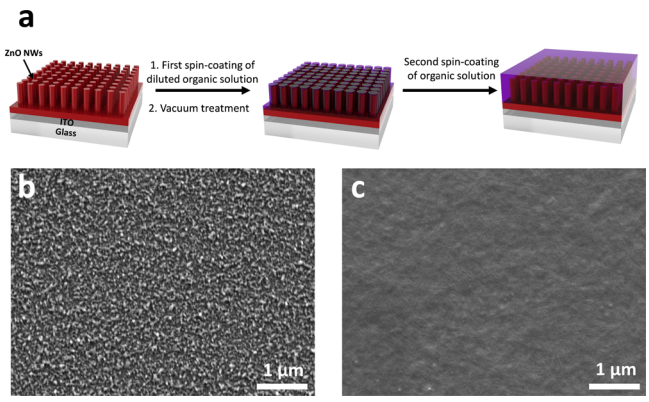

Figure 4. (a) Schematic illustration of the VADC process. SEM images of the P3HT:PCBM-based hybrid film (b) after vacuum treatment during the VADC process and (c) after the VADC process.

ZnO NW layer and then vacuum-treated to improve the infiltration. This was followed by a second spin-coating method of a more concentrated (same concentration of the conventional single spin-coating method) organic solution (see Experimental Section). Figure 4b shows an SEM image of the film that was vacuum-treated after coating of the diluted organic solution on ZnO NWs. The thin organic layer effectively filled the interspatial voids between the organic layer and the ZnO NW layer by vacuum treatment. After the secondary spin-coating treatment, the organic layer fully covered the ZnO NW arrays, forming a smooth surface (Figure 4c). To investigate the morphologies of the hybrid films, atomic force microscopy (AFM) analysis was performed (Figure S1, Supporting Information). The average surface roughness of the VADC-based films was 8 nm, which was smaller than that (13 nm) of the single spin-coating-based film. Contact angle measurement results using a P3HT:PCBM solution (2 μL droplet) onto only ZnO NWs and ZnO NWs with vacuum-treated single-coated P3HT:PCBM layer are shown in Figure S2 (Supporting Information). Both only ZnO NWs (contact angle = 11°) and ZnO NWs with a vacuum-treated single-coated P3HT:PCBM layer (contact angle = 15°) showed high affinity with the P3HT:PCBM solution. Only ZnO NWs showed slightly better affinity with the organic solution than ZnO NWs with a vacuum-treated single-coated P3HT:PCBM layer, but there was no significant difference. The VADC method first forms a thin organic photoactive layer on the lower part of the ZnO NWs by a conventional coating method and a dense organic layer between the ZnO NWs by coating the photoactive layer solution after vacuum treatment. Therefore, this small affinity difference between these substrates and organic solutions may not have a significant effect on the formation of the compact hybrid films. The hybrid films prepared by the VADC method exhibited higher

DOI: 10.1021/acsomega.9b00778
ACS Omega 2019, 4, 9996−10002

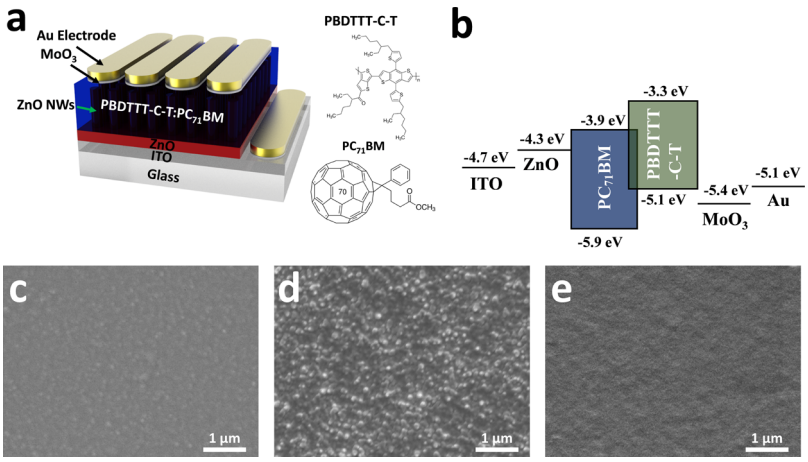

Figure 5. (a) Schematic image of the PBDTTT-C-T:$PC_{71}BM$-based HPV with molecular structures of PBDTTT-C-T and $PC_{71}BM$. (b) Schematic energy level diagram of the PBDTTT-C-T:$PC_{71}BM$-based HPV. (c, d) SEM images (c) before and (d) after vacuum processing of the PBDTTT-C-T:$PC_{71}BM$-based hybrid film fabricated by the conventional spin-coating method. (e) SEM image of the PBDTTT-C-T:$PC_{71}BM$-based hybrid film after the VADC process.

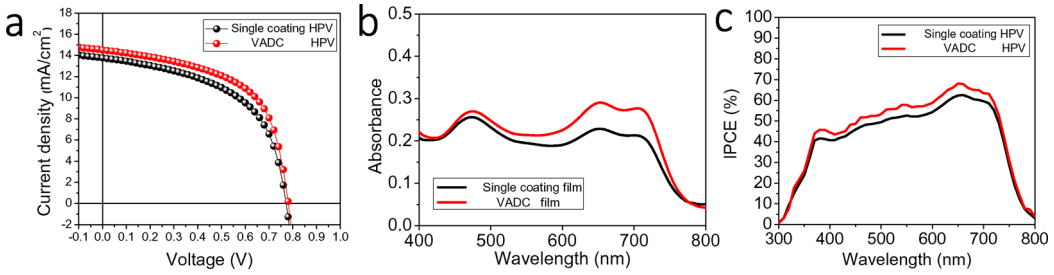

Figure 6. (a) $J-V$ characteristics of PBDTTT-C-T:$PC_{71}BM$-based HPVs fabricated using the single spin-coating and VADC methods under white-light illumination (AM 1.5G, 100 mW/cm^2). (b) UV–vis absorption spectra of PBDTTT-C-T:$PC_{71}BM$-based hybrid films fabricated using the single spin-coating and VADC methods. (c) IPCE characteristics of PBDTTT-C-T:$PC_{71}BM$-based HPVs fabricated using the single spin-coating and VADC methods.

light absorption characteristics compared with the hybrid films prepared by the conventional single spin-coating process due to the formation of a compact film without interspatial voids and smooth surface (Figure S3, Supporting Information). In conjunction with the perfect infiltration of P3HT:PCBM into the densely packed ZnO NW arrays, the smooth surface morphology of the P3HT:PCBM layer obtained using the VADC method enhanced the PCE in HPVs (vide infra).

The current density–voltage ($J-V$) characteristics and P3HT:PCBM-based HPV performance parameters are summarized in Figure 3a and Table 1, respectively. The HPVs fabricated using the VADC method showed an improved PCE (~11% increase from 3.25 to 3.62%) over HPVs fabricated using the single spin-coating process. The short-circuit current density (J_{sc}), open-circuit voltage (V_{oc}), and fill factor (FF) values of HPVs fabricated by VADC were enhanced compared with HPVs fabricated by the single spin-coating method. The improvements in V_{oc} and FF were attributed to an increase in shunt resistance (R_{sh}) and a reduction in series resistance (R_s), respectively. The increase in J_{sc} was due to a more efficient photogenerated charge separation and a reduction in R_s. The changes in R_{sh}, R_s, and the photogenerated charge collection are all due to a higher level of organic layer infiltration, leading to a denser HPV device. The incident photon-to-charge carrier efficiency (IPCE) characteristics of the HPVs are shown in Figure S4 (Supporting Information). By applying the VADC method, the IPCEs of the HPVs increased between the wavelengths of 300 and 700 nm. This result indicates a significant improvement in the infiltration of the organic layer into ZnO NWs, leading to an improvement in electrical contact between them.

Moreover, it has been confirmed that VADC is also effective for improving the performance of PBDTTT-C-T:$PC_{71}BM$-based HPVs. PBDTTT-C-T is another promising low band gap polymer for high-performance OPVs. In the case of the PBDTTT-C-T:$PC_{71}BM$-based HPVs, the organic solution was coated and then vacuumed at room temperature without post-annealing to remove the solvent due to the thermal vulnerability of PBDTTT-C-T. A schematic image with molecular structures of organic semiconductors and energy diagram of the PBDTTT-C-T:$PC_{71}BM$-based HPVs are presented in Figure 5a,b, respectively (band gaps of PBDTTT-C-T and $PC_{71}BM$ are ~1.8 and ~2 eV, respectively).[44,47] Figure 5c,d shows the SEM images before and after vacuum processing of the PBDTTT-C-T:$PC_{71}BM$-based hybrid film fabricated by the conventional spin-coating method. Similar to the case of P3HT:PCBM films, the interspatial voids between the organic layer and the ZnO NW layer were greatly reduced by vacuum treatment and showed the sinkage of the organic layer. The VADC method yielded the organic layer with a smooth surface on the ZnO NW arrays (Figure 5e). The average surface roughness (9 nm) of the VADC-based hybrid film was less than that (15 nm) of the single spin-coating-based hybrid film (Figure S5, Supporting

DOI: 10.1021/acsomega.9b00778
ACS Omega 2019, 4, 9996–10002

Table 2. Photovoltaic Performance Parameters of the PBDTTT-C-T:$PC_{71}BM$-Based HPVs Fabricated Using the Single Spin-Coating and VADC Methods

coating methods	J_{sc} (mA/cm^2)	V_{oc} (V)	FF (%)	R_{sh} (KΩ cm^2)	R_s (Ω cm^2)	PCE_{max} (PCE_{av}) (%)
single coating	13.8	0.77	53.9	2.27	18.4	5.73 (5.66)[a]
VADC	14.5	0.78	57.6	2.52	17.8	6.53 (6.24)

[a]Average values are based on the testing of five devices.

Information). Furthermore, contact angle measurement results using a PBDTTT-C-T:$PC_{71}BM$ solution onto only ZnO NWs and ZnO NWs with a vacuum-treated single-coated PBDTTT-C-T:$PC_{71}BM$ layer also showed similar tendency to the P3HT:PCBM system as shown in Figure S6 (Supporting Information). Contact angle values of only ZnO NWs and ZnO NWs with a vacuum-treated single-coated PBDTTT-C-T:$PC_{71}BM$ layer were 10° and 11°, respectively. The $J-V$ characteristics and PBDTTT-C-T:$PC_{71}BM$-based HPV performance parameters are summarized in Figure 6a and Table 2, respectively. The PCEs of the PBDTTT-C-T:$PC_{71}BM$-based HPVs improved by 14% (from 5.73 to 6.53%) using the VADC method due to the enhancement of J_{sc}, V_{oc}, and FF, which is consistent with the results observed from the HPVs based on P3HT:PCBM. The hybrid film fabricated by the VADC method also showed enhanced light absorption characteristics compared with the hybrid film fabricated by the conventional single spin-coating method (Figure 6b). Moreover, as shown in Figure 6c, the IPCE characteristics of the VADC-based HPVs were enhanced over the absorption range between the wavelengths of 300 and 800 nm compared with the single spin-coating-based HPVs. This is due to the perfect infiltration of PBDTTT-C-T:$PC_{71}BM$ into the densely packed ZnO NW arrays and the formation of the smooth surface morphology of the HPV devices.

3. CONCLUSIONS

In summary, we have demonstrated the fabrication of HPVs based on a ZnO NW/organic hybrid thin film adjoined to a compact ZnO hole-blocking layer by means of the newly proposed VADC method. The VADC method significantly improved the PCE of P3HT:PCBM- and PBDTTT-C-T:$PC_{71}BM$-based HPVs (by 11 and 14%, respectively) compared with the HPVs fabricated by the conventional single spin-coating process. The VADC method resulted in the efficient infiltration of the organic semiconductors into the densely packed ZnO NW arrays. Our studies provide an effective method to achieve perfect interfacial contact between organic and inorganic nanostructures, resulting in the development of high-performance HPV systems. We expect that these studies can be utilized to enhance the performance of a wide range of HPVs.

4. EXPERIMENTAL SECTION

4.1. Device Fabrication. The devices were fabricated using an inverted structure of ITO glass/compact ZnO/ZnO NWs/P3HT:PCBM or PBDTTT-C-T:$PC_{71}BM$/MoO_3/Au. The ITO glasses (EM index) were cleaned by sequential ultrasonic treatment in detergent, deionized (DI) water, acetone, and isopropanol for 15 min. The ITO glasses were then treated by UV−ozone (O_3) for 20 min. The compact ZnO buffer layer was prepared by spin-coating a diethylzinc solution (0.37 M, obtained by adding 2 mL of a 1.1 M diethylzinc solution in toluene to 4 mL of dry tetrahydrofuran, Merck) on the ITO substrate and then baked at 110 °C for 10 min. The ZnO NWs were hydrothermally grown in aqueous solution. To prepare the growing solution of the ZnO NWs, equimolar amounts (25×10^{-3} M) of $Zn(NO_3)_2{\cdot}xH_2O$ (99.9%, Sigma-Aldrich) and hexamethylenetetramine (HMTA) (≥99.0%, Sigma-Aldrich) were dispersed in DI water by sonication. Then, the compact ZnO buffer layer-deposited ZnO/ITO/glass substrates were floated on the surface of the growing solution. The length and diameter of the ZnO NWs were varied by controlling the growth time. After finishing the growing ZnO NWs within 30 min, the surface of the ZnO NWs was rinsed with DI water to remove excess ions and aggregated ZnO precipitates. The photosensitive blend layer was prepared using the single spin-coating or VADC method for tuning morphology. For the single spin-coating method, an ODCB solution of P3HT:PCBM (EM index) (15 mg, 12 mg/mL) or PBDTTT-C-T:$PC_{71}BM$ (8 mg, 12 mg/mL) with a 3% (v/v) ratio of 1,8-diiodooctane (DIO, EM index) was spin-coated at 600 rpm for 60 s onto the UV−O_3-treated ZnO NW grown cells. The P3HT:PCBM cells were subsequently annealed at 110 °C for 20 min, and the PBDTTT-C-T:$PC_{71}BM$ cells were placed in a vacuum chamber for 20 min (~10^{-2} torr). For the VADC method, the active layer was spin-coated using a double coating process. In the first coating process, a 10-fold diluted solution of either P3HT:PCBM or PBDTTT-C-T:$PC_{71}BM$ was spin-coated onto the UV−O_3-treated ZnO NW grown cells, and the whole sample was placed in a vacuum chamber for 20 min (~10^{-2} torr). Subsequently, the undiluted organic solution was re-spin-coated onto the cells at 600 rpm for 60 s. The P3HT:PCBM cells were annealed at 110 °C for 20 min, and the PBDTTT-C-T:$PC_{71}BM$ cells were placed in a vacuum chamber for 20 min (~10^{-2} torr). Finally, a 5 nm-thick MoO_3 layer and 130 nm-thick Au layer were thermally deposited consecutively onto the photoactive layer under vacuum (~10^{-6} torr). The area of the Au electrode defined the active area of the device as 10 mm^2.

4.2. Measurement. The $J-V$ characteristics of HPVs were measured using the Keithley 2400A Source Measure Unit. The solar cell performance was evaluated using the Air Mass 1.5 Global (AM 1.5 G) solar simulator with an irradiation intensity of 100 mW cm^{-2}. The absorption and IPCE spectra were obtained using a spectrophotometer (JASCO V0670) and QE/IPCE measurement system (QEX7 Serial #90), respectively. IPCE measurements were obtained using a PV measurement OE system by applying monochromatic light from a xenon lamp under ambient conditions. The monochromatic light intensity was calibrated using a Si photodiode with a 100 Hz cutoff. The SEM images were obtained using a Hitachi cold SEM microscope. The AFM images were obtained using the Veeco AFM microscope and Park System NX10 in tapping mode. The UV−vis absorption spectra were measured on a spectrophotometer.

DOI: 10.1021/acsomega.9b00778
ACS Omega 2019, 4, 9996−10002

■ ASSOCIATED CONTENT

Supporting Information

The Supporting Information is available free of charge on the ACS Publications website at DOI: 10.1021/acsomega.9b00778.

AFM images of P3HT:PCBM-based hybrid films fabricated using the single spin-coating and VADC methods, UV−vis absorption spectra of P3HT:PCBM-based hybrid films fabricated using the single spin-coating and VADC methods, IPCE characteristics of P3HT:PCBM-based HPVs fabricated using the single spin-coating and VADC methods, and AFM images of PBDTTT-C-T:$PC_{71}BM$-based hybrid films fabricated using the single spin-coating and VADC methods (PDF)

■ AUTHOR INFORMATION

Corresponding Authors

*E-mail: hyunhko@unist.ac.kr (H.K).
*E-mail: joonhoh@snu.ac.kr (J.H.O.).

ORCID

Hyunhyub Ko: 0000-0003-2111-6101
Joon Hak Oh: 0000-0003-0481-6069

Present Address

[‖]Y.H.L. is a researcher of the Center for Advanced Soft Electronics and currently works as a visiting researcher at Seoul National University.

Author Contributions

[§]Y.H.L. and M.H. have contributed equally.

Notes

The authors declare no competing financial interest.

■ ACKNOWLEDGMENTS

This work was supported by the National Research Foundation of Korea (NRF) grant (no. 2017R1E1A1A01074090, 2018M3C1B2087541) and the Center for Advanced Soft-Electronics funded by the Ministry of Science, ICT of Korea as Global Frontier Project (CASE-2011-0031628).

■ REFERENCES

(1) Che, X.; Li, Y.; Qu, Y.; Forrest, S. R. High fabrication yield organic tandem photovoltaics combining vacuum- and solution-processed subcells with 15% efficiency. *Nat. Energy* **2018**, *3*, 422−427.
(2) Yan, C.; Barlow, S.; Wang, Z.; Yan, H.; Jen, A. K. Y.; Marder, S. R.; Zhan, X. Non-fullerene acceptors for organic solar cells. *Nat. Rev. Mater.* **2018**, *3*, 18003.
(3) Elumalai, N. K.; Uddin, A. Open circuit voltage of organic solar cells: an in-depth review. *Energy Environ. Sci.* **2016**, *9*, 391−410.
(4) Hedley, G. J.; Ruseckas, A.; Samuel, I. D. W. Light Harvesting for Organic Photovoltaics. *Chem. Rev.* **2017**, *117*, 796−837.
(5) Wadsworth, A.; Moser, M.; Marks, A.; Little, M. S.; Gasparini, N.; Brabec, C. J.; Baran, D.; McCulloch, I. Critical review of the molecular design progress in non-fullerene electron acceptors towards commercially viable organic solar cells. *Chem. Soc. Rev.* **2019**, *48*, 1596−1625.
(6) Huang, H.; Yang, L.; Sharma, B. Recent advances in organic ternary solar cells. *J. Mater. Chem. A* **2017**, *5*, 11501−11517.
(7) Li, H.; Zhao, Y.; Fang, J.; Zhu, X.; Xia, B.; Lu, K.; Wang, Z.; Zhang, J.; Guo, X.; Wei, Z. Improve the Performance of the All-Small-Molecule Nonfullerene Organic Solar Cells through Enhancing the Crystallinity of Acceptors. *Adv. Energy Mater.* **2018**, *8*, 1702377.
(8) Tang, Z.; Tress, W.; Inganäs, O. Light trapping in thin film organic solar cells. *Mater. Today* **2014**, *17*, 389−396.
(9) Lee, Y. H.; Lee, T. K.; Song, I.; Yu, H.; Lee, J.; Ko, H.; Kwak, S. K.; Oh, J. H. Boosting the Performance of Organic Optoelectronic Devices Using Multiple-Patterned Plasmonic Nanostructures. *Adv. Mater.* **2016**, *28*, 4976−4982.
(10) Chidichimo, G.; Filippelli, L. Organic Solar Cells: Problems and Perspectives. *Int. J. Photoenergy* **2010**, *2010*, 123534.
(11) Sha, W. E. I.; Li, X.; Choy, W. C. H. Breaking the Space Charge Limit in Organic Solar Cells by a Novel Plasmonic-Electrical Concept. *Sci. Rep.* **2014**, *4*, 6236.
(12) Hau, S. K.; Yip, H.-L.; Baek, N. S.; Zou, J.; O'Malley, K.; Jen, A. K. Y. Air-stable inverted flexible polymer solar cells using zinc oxide nanoparticles as an electron selective layer. *Appl. Phys. Lett.* **2008**, *92*, 253301.
(13) Hoppe, H.; Sariciftci, N. S. Organic solar cells: An overview. *J. Mater. Res.* **2004**, *19*, 1924−1945.
(14) Adikaari, A. A. D. T.; Dissanayake, D. M. N. M.; Silva, S. R. P. Organic-Inorganic Solar Cells: Recent Developments and Outlook. *IEEE J. Sel. Top. Quantum Electron.* **2010**, *16*, 1595−1606.
(15) Lu, L.; Zheng, T.; Wu, Q.; Schneider, A. M.; Zhao, D.; Yu, L. Recent Advances in Bulk Heterojunction Polymer Solar Cells. *Chem. Rev.* **2015**, *115*, 12666−12731.
(16) Shen, X.; Sun, B.; Liu, D.; Lee, S.-T. Hybrid Heterojunction Solar Cell Based on Organic−Inorganic Silicon Nanowire Array Architecture. *J. Am. Chem. Soc.* **2011**, *133*, 19408−19415.
(17) Yu, P.; Tsai, C.-Y.; Chang, J.-K.; Lai, C.-C.; Chen, P.-H.; Lai, Y.-C.; Tsai, P.-T.; Li, M.-C.; Pan, H.-T.; Huang, Y.-Y.; Wu, C.-I.; Chueh, Y.-L.; Chen, S.-W.; Du, C.-H.; Horng, S.-F.; Meng, H.-F. 13% Efficiency Hybrid Organic/Silicon-Nanowire Heterojunction Solar Cell via Interface Engineering. *ACS Nano* **2013**, *7*, 10780−10787.
(18) Xu, W.; Tan, F.; Liu, X.; Zhang, W.; Qu, S.; Wang, Z.; Wang, Z. Efficient Organic/Inorganic Hybrid Solar Cell Integrating Polymer Nanowires and Inorganic Nanotetrapods. *Nanoscale Res. Lett.* **2017**, *12*, 11.
(19) Ren, S.; Chang, L.-Y.; Lim, S.-K.; Zhao, J.; Smith, M.; Zhao, N.; Bulović, V.; Bawendi, M.; Gradečak, S. Inorganic−Organic Hybrid Solar Cell: Bridging Quantum Dots to Conjugated Polymer Nanowires. *Nano Lett.* **2011**, *11*, 3998−4002.
(20) Um, H.-D.; Choi, D.; Choi, A.; Seo, J. H.; Seo, K. Embedded Metal Electrode for Organic−Inorganic Hybrid Nanowire Solar Cells. *ACS Nano* **2017**, *11*, 6218−6224.
(21) Müller-Buschbaum, P.; Thelakkat, M.; Fässler, T. F.; Stutzmann, M. Hybrid Photovoltaics − from Fundamentals towards Application. *Adv. Energy Mater.* **2017**, *7*, 1700248.
(22) Huang, J.; Yin, Z.; Zheng, Q. Applications of ZnO in organic and hybrid solar cells. *Energy Environ. Sci.* **2011**, *4*, 3861−3877.
(23) Wei, B.; Pan, S.; Wang, T.; Tian, Z.; Chen, G.; Xu, T. Solution-processed Ag-nanowire/ZnO-nanoparticle composite transparent electrode for flexible organic solar cells. *Nanotechnology* **2016**, *27*, 505208.
(24) Chang, S.; Park, H.; Cheng, J. J.; Rekemeyer, P. H.; Gradečak, S. Improved efficiency in organic/inorganic hybrid solar cells by interfacial modification of ZnO nanowires with small molecules. *J. Phys. D* **2014**, *47*, 394016.
(25) Cheng, J. J.; Nicaise, S. M.; Berggren, K. K.; Gradečak, S. Dimensional Tailoring of Hydrothermally Grown Zinc Oxide Nanowire Arrays. *Nano Lett.* **2016**, *16*, 753−759.
(26) Bagga, S.; Akhtar, J.; Mishra, S. Synthesis and applications of ZnO nanowire: A review. *AIP Conf. Proc.* **2018**, *1989*, No. 020004.
(27) Shih, P.-H.; Wu, S. Y. Growth Mechanism Studies of ZnO Nanowires: Experimental Observations and Short-Circuit Diffusion Analysis. *Nanomaterials* **2017**, *7*, 188.
(28) Zhang, Y.; Ram, M. K.; Stefanakos, E. K.; Goswami, D. Y. Synthesis, Characterization, and Applications of ZnO Nanowires. *J. Nanomater.* **2012**, *2012*, 20.
(29) Ha, M.; Lim, S.; Park, J.; Um, D.-S.; Lee, Y.; Ko, H. Bioinspired Interlocked and Hierarchical Design of ZnO Nanowire Arrays for Static and Dynamic Pressure-Sensitive Electronic Skins. *Adv. Funct. Mater.* **2015**, *25*, 2841−2849.

DOI: 10.1021/acsomega.9b00778
ACS Omega 2019, 4, 9996−10002

(30) Lim, S.; Um, D.-S.; Ha, M.; Zhang, Q.; Lee, Y.; Lin, Y.; Fan, Z.; Ko, H. Broadband omnidirectional light detection in flexible and hierarchical ZnO/Si heterojunction photodiodes. *Nano Res.* **2017**, *10*, 22−36.
(31) Olson, D. C.; Lee, Y. J.; White, M. S.; Kopidakis, N.; Shaheen, S. E.; Ginley, D. S.; Voigt, J. A.; Hsu, J. W. P. Effect of polymer processing on the performance of poly(3-hexylthiophene)/ZnO nanorod photovoltaic devices. *J. Phys. Chem. C* **2007**, *111*, 16640−16645.
(32) Ravirajan, P.; Peiró, A. M.; Nazeeruddin, M. K.; Graetzel, M.; Bradley, D. D. C.; Durrant, J. R.; Nelson, J. Hybrid polymer/zinc oxide photovoltaic devices with vertically oriented ZnO nanorods and an amphiphilic molecular interface layer. *J. Phys. Chem. B* **2006**, *110*, 7635−7639.
(33) Yang, P.; Yan, H.; Mao, S.; Russo, R.; Johnson, J.; Saykally, R.; Morris, N.; Pham, J.; He, R.; Choi, H. J. Controlled growth of ZnO nanowires and their optical properties. *Adv. Funct. Mater.* **2002**, *12*, 323−331.
(34) Tong, F.; Kim, K.; Martinez, D.; Thapa, R.; Ahyi, A.; Williams, J.; Kim, D. J.; Lee, S.; Lim, E.; Lee, K. K.; Park, M. Flexible organic/inorganic hybrid solar cells based on conjugated polymer and ZnO nanorod array. *Semicond. Sci. Technol.* **2012**, *27*, 105005.
(35) Yi, G.-C.; Wang, C.; Park, W. I. ZnO nanorods: synthesis, characterization and applications. *Semicond. Sci. Technol.* **2005**, *20*, S22−S34.
(36) Zhang, Q.; Dandeneau, C. S.; Zhou, X.; Cao, G. ZnO Nanostructures for Dye-Sensitized Solar Cells. *Adv. Mater.* **2009**, *21*, 4087−4108.
(37) Garnier, F. Hybrid organic-on-inorganic photovoltaic devices. *J. Opt. A* **2002**, *4*, S247−S251.
(38) Kim, T.; Jeon, J. H.; Han, S.; Lee, D. K.; Kim, H.; Lee, W.; Kim, K. Organic-inorganic hybrid tandem multijunction photovoltaics with extended spectral response. *Appl. Phys. Lett.* **2011**, *98*, 183503.
(39) Li, Z.; Zhang, X.; Lu, G. Dipole-Assisted Charge Separation in Organic-Inorganic Hybrid Photovoltaic Heterojunctions: Insight from First-Principles Simulations. *J. Phys. Chem. C* **2012**, *116*, 9845−9851.
(40) Neyshtadt, S.; Jahnke, J. P.; Messinger, R. J.; Rawal, A.; Peretz, T. S.; Huppert, D.; Chmelka, B. F.; Frey, G. L. Understanding and Controlling Organic-Inorganic Interfaces in Mesostructured Hybrid Photovoltaic Materials. *J. Am. Chem. Soc.* **2011**, *133*, 10119−10133.
(41) He, Z.; Zhong, C.; Su, S.; Xu, M.; Wu, H.; Cao, Y. Enhanced power-conversion efficiency in polymer solar cells using an inverted device structure. *Nat. Photonics* **2012**, *6*, 591.
(42) Chou, C.-Y.; Huang, J.-S.; Wu, C.-H.; Lee, C.-Y.; Lin, C.-F. Lengthening the polymer solidification time to improve the performance of polymer/ZnO nanorod hybrid solar cells. *Sol. Energy Mater. Sol. Cells* **2009**, *93*, 1608−1612.
(43) Olson, D. C.; Piris, J.; Collins, R. T.; Shaheen, S. E.; Ginley, D. S. Hybrid photovoltaic devices of polymer and ZnO nanofiber composites. *Thin Solid Films* **2006**, *496*, 26−29.
(44) Jagadamma, L. K.; Al-Senani, M.; El-Labban, A.; Gereige, I.; Ngongang Ndjawa, G. O.; Faria, J. C. D.; Kim, T.; Zhao, K.; Cruciani, F.; Anjum, D. H.; McLachlan, M. A.; Beaujuge, P. M.; Amassian, A. Polymer Solar Cells with Efficiency >10% Enabled via a Facile Solution-Processed Al-Doped ZnO Electron Transporting Layer. *Adv. Energy Mater.* **2015**, *5*, 1500204.
(45) Cheng, P.; Li, G.; Zhan, X.; Yang, Y. Next-generation organic photovoltaics based on non-fullerene acceptors. *Nat. Photonics* **2018**, *12*, 131−142.
(46) Berger, P. R.; Kim, M. Polymer solar cells: P3HT:PCBM and beyond. *J. Renewable Sustainable Energy* **2018**, *10*, No. 013508.
(47) Hsu, C.-H.; Lai, C.-C.; Chen, L.-C.; Chan, P.-S. Enhanced Performance of Dye-Sensitized Solar Cells with Graphene/ZnO Nanoparticles Bilayer Structure. *J. Nanomater.* **2014**, *2014*, 4.
(48) Page, Z. A.; Liu, Y.; Duzhko, V. V.; Russell, T. P.; Emrick, T. Fulleropyrrolidine interlayers: Tailoring electrodes to raise organic solar cell efficiency. *Science* **2014**, *346*, 441−444.
(49) Yeom, H. R.; Heo, J.; Kim, G.-H.; Ko, S.-J.; Song, S.; Jo, Y.; Kim, D. S.; Walker, B.; Kim, J. Y. Optimal top electrodes for inverted polymer solar cells. *Phys. Chem. Chem. Phys.* **2015**, *17*, 2152−2159.
(50) Huang, J. S.; Chou, C. Y.; Lin, C. F. Enhancing performance of organic-inorganic hybrid solar cells using a fullerene interlayer from all-solution processing. *Sol. Energy Mater. Sol. Cells* **2010**, *94*, 182−186.
(51) Baeten, L.; Conings, B.; Boyen, H. G.; D'Haen, J.; Hardy, A.; D'Olieslaeger, M.; Manca, J. V.; Van Bael, M. K. Towards Efficient Hybrid Solar Cells Based on Fully Polymer Infiltrated ZnO Nanorod Arrays. *Adv. Mater.* **2011**, *23*, 2802−2805.

DOI: 10.1021/acsomega.9b00778
ACS Omega 2019, 4, 9996−10002